Electrical Power and Energy Systems 67 (2015) 101–113

Contents lists available at ScienceDirect

Electrical Power and Energy Systems

journal homepage: www.elsevier.com/locate/ijepes

# Simultaneous capacity optimization of distributed generation and storage in medium voltage microgrids

E.E. Sfikas, Y.A. Katsigiannis, P.S. Georgilakis *

*School of Electrical and Computer Engineering, National Technical University of Athens (NTUA), GR 15780 Athens, Greece*

ARTICLE INFO

*Article history:*
Received 3 September 2014
Received in revised form 10 October 2014
Accepted 15 November 2014

*Keywords:*
Distributed generation
Energy storage
Microgrid
Power system optimization
Power system planning

ABSTRACT

The main contribution of this paper is that it introduces the simultaneous capacity optimization of distributed generation (DG) and storage in grid-connected and standalone microgrids. Hourly planning of the microgrid operation is performed, taking into consideration certain characteristics of the grid and the units, together with local climate data that impact the output of non-dispatchable renewable resources. The proposed formulation constitutes a nonlinear programming problem that is solved by a sequential quadratic programming method. The model is then applied for a test case microgrid, examining both grid-connected and standalone operation. Two alternative objective functions are investigated: (a) the minimization of the total annual energy losses (TAEL), and (b) the minimization of the cost of energy (COE). Depending on the considered objective function, the results show a significant reduction in either the TAEL or the COE for the grid-connected microgrid, as well as a higher degree of independence from the main grid, which provides the capability of standalone operation. In this case, the energy storage systems play the most crucial role. Consequently, the results prove the positive effect of the proposed simultaneous capacity optimization of energy storage and DG in the cases of grid-connected and standalone microgrid operation.



## Introduction

Microgrids are state-of-the-art low and medium voltage power distribution networks consisting of distributed generation units, storage devices and flexible loads, operated connected to the main power network or islanded, in a controlled, coordinated way [1]. Rapid connection of renewable and non-renewable distributed generation (DG) resources to the distribution network has been observed around the world, and the reasons to implement DG range from energy efficiency or rational use of energy, to deregulation or competitive energy policy, diversification of energy resources, capability to develop renewable energy sources, reduction of greenhouse gases and alleviation of global warming, reduction of on-peak operating cost, availability of modular DG plants, ease of finding sites for smaller generators, shorter construction times, lower capital costs of smaller DG plants, network upgrade delay or deferral, and closeness of DG plant to large loads that leads to transmission cost reduction [2–6]. Microgrids coordinate distributed energy resources in a consistently more decentralized way, thereby reducing the control burden on the grid and permitting them to provide their full benefits. A microgrid operates safely and efficiently within its local distribution network, but it is also capable of standalone operation, where the role of energy storage is more critical, compared to the grid-connected microgrid case [4].

The optimal DG placement (ODGP) problem in power distribution networks has attracted a lot of research efforts in the last 20 years [2]. Methods applied to solve the ODGP include adapted analytical expressions [7], hierarchical agglomerative clustering algorithm [8], genetic algorithm [9], memetic algorithm [10], and fireworks algorithm – a swarm intelligence based optimization method [11]. More specifically, an analytical method is proposed for the determination of the optimal size and power factor of dispatchable and nondispatchable DG units in distribution networks [7]. DG siting and sizing is formulated as a multiobjective optimization problem, which is solved by a hierarchical agglomerative clustering algorithm that overcomes the dependency of existing DG planning methods on global preference information [8]. A genetic algorithm method, based on average daily load and power production curves, is developed to determine the optimal locations and sizes of three types of DG units (solar park, wind farm, and power station that does not depend on an intermittent primary energy source) [9]. The determination of the optimal location and size of DG units and capacitors in distribution networks considering the voltage stability index is proposed in [10]. The optimal

* Corresponding author. Tel.: +30 210 772 4378; fax: +30 210 772 3659.
*E-mail address:* pgeorg@power.ece.ntua.gr (P.S. Georgilakis).

http://dx.doi.org/10.1016/j.ijepes.2014.11.009
0142-0615/

**Nomenclature**

*Abbreviations*

| | |
|---|---|
| BSS | battery storage system, which mainly consists of a power conditioning system and a storage unit |
| CRF | capital recovery factor |
| PCS | power conditioning system |

*Indicators*

| | |
|---|---|
| $i$,$k$ | bus number indicators |
| $j$ | state number indicator |
| $t$ | hour indicator |

*Parameters*

| | |
|---|---|
| $B_{ik}$ | imaginary part of the element of the bus admittance matrix that refers to the line between buses $i$ and $k$ |
| $Bio_a$ | biomass fuel cost parameter $a$ |
| $Bio_b$ | biomass fuel cost parameter $b$ |
| $C_{exch}$ | cost of energy exchanged through the substation |
| $CI_b$ | biomass units investment cost |
| $CI_e$ | batteries investment cost |
| $CI_s$ | photovoltaics investment cost |
| $CI_w$ | wind turbines investment cost |
| $CM_b$ | biomass units annual maintenance cost |
| $CM_e$ | batteries annual maintenance cost |
| $CM_s$ | photovoltaics annual maintenance cost |
| $CM_w$ | wind turbines annual maintenance cost |
| $Days_j$ | total days of the year that state $j$ represents |
| $eff$ | battery efficiency |
| $G_{ik}$ | real part of the element of the bus admittance matrix that refers to the line between buses $i$ and $k$ |
| $load_{j,t}$ | percentage of rated load at all buses at hour $t$ of state $j$ |
| $P_{bus\ i}$ | rated active power of load at bus $i$ |
| $P_{load,total}$ | maximum total active power demand |
| $Poss_j$ | possibility of occurrence of state $j$ |
| $Q_{bus\ i}$ | rated reactive power of load at bus $i$ |
| $Q_{load,total}$ | maximum total reactive power demand |
| $solar_{j,t}$ | percentage of rated power produced by the photovoltaics at hour $t$ of state $j$ |
| $v_{\max}$ | maximum voltage magnitude |
| $v_{\min}$ | minimum voltage magnitude |
| $wind_{j,t}$ | percentage of rated power produced by the wind turbines at hour $t$ of state $j$ |
| $\delta_{\max}$ | maximum voltage angle |
| $\delta_{\min}$ | minimum voltage angle |
| $\phi_b$ | power factor angle of biomass units |
| $\phi_e$ | power factor angle of BSS |
| $\phi_s$ | power factor angle of photovoltaics |
| $\phi_w$ | power factor angle of wind turbines |

*Variables*

| | |
|---|---|
| $E_i$ | energy storage capacity of the battery of bus $i$ |
| $Ech_{j,i}$ | energy charged by the battery of bus $i$, during the whole state $j$ |
| $Edis_{j,i}$ | energy discharged by the battery of bus $i$, during the whole state $j$ |
| $P_i$ | active power capacity of the battery of bus $i$ |
| $Pb_{j,i}$ | biomass output power at bus $i$, at state $j$ |
| $Pbought_{j,t,1}$ | real power injected by the substation at hour $t$ of state $j$ for the case of grid-connected microgrid; this means that $Pbought_{j,t,1}$ is the power the microgrid buys from the transmission network |
| $Pch_{j,t,i}$ | active power charged by the battery of bus $i$, at hour $t$ of state $j$ |
| $Pdis_{j,t,i}$ | active power discharged by the battery of bus $i$, at hour $t$ of state $j$ |
| $Pin_{j,t,1}$ | real power injected or absorbed by the substation at hour $t$ of state $j$ for the case of grid-connected microgrid |
| $Ps_i$ | rated solar power at bus $i$ |
| $Psold_{j,t,1}$ | real power absorbed by the substation at hour $t$ of state $j$ for the case of grid-connected microgrid; this means that $Psold_{j,t,1}$ is the power the microgrid sells to the transmission network |
| $Pw_i$ | rated wind power at bus $i$ |
| $Qch_{j,t,i}$ | reactive power charged by the battery of bus $i$, at hour $t$ of state $j$ |
| $Qdis_{j,t,i}$ | reactive power discharged by the battery of bus $i$, at hour $t$ of state $j$ |
| $Qin_{j,t,1}$ | reactive power injected by the substation at hour $t$ of state $j$ for the case of grid-connected microgrid |
| $v_{j,t,i}$ | voltage magnitude at bus $i$, at hour $t$ of state $j$ |
| $\delta_{j,t,i}$ | voltage angle at bus $i$, at hour $t$ of state $j$ |

location and size of DG units and the optimal network reconfiguration are simultaneously determined in [11].

Methods applied to solve the ODGP under uncertainties include point estimate method embedded genetic algorithm [3], plant growth simulation algorithm with probabilistic optimal power flow [12], particle swarm optimization and Monte Carlo simulation [13], and artificial neural networks [14]. The work [12] introduces the optimal location and size of distributed wind generation units for a smart distribution network operating under active management mode. A multiobjective method is proposed to determine the optimal location and size of DG units considering the uncertainty of the market price as well as the effect of load models [13]. Artificial neural networks are proposed to determine the optimal location and size of DG units considering load uncertainty and DG penetration levels [14]. A systematic qualitative assessment of the state of the art models and methods applied to the ODGP together with the contribution of all of the reviewed ODGP works can be found in [2].

The optimal location and size of energy storage systems (ESS) in low voltage networks is determined by genetic algorithm and simulated annealing in [15]. The optimal placement and sizing of battery switching station units is solved by artificial bee colony algorithm in [16]. A methodology for the optimal allocation of battery storage system (BSS) in distribution networks with a high penetration of wind energy is proposed in [17]. A method for finding the optimal size of BSS for primary frequency control of a microgrid is developed in [18]. A statistical model is used to determine the capacity of battery–superconductor hybrid energy storage system in autonomous microgrid [19]. The state-of-the-art of research on optimum sizing of standalone hybrid solar–wind power generation systems with battery storage can be found in [20].

From the above survey, it is obvious that sufficient work has been done in the area of sizing of DG and BSS. However, the problem of simultaneous sizing of BSS and DG (dispatchable and non-dispatchable) in grid-connected and standalone microgrids has not been tackled yet.

This paper introduces the simultaneous capacity optimization of distributed generation and battery storage in microgrids, considering their two possible operation states, namely, grid-connected or standalone (autonomous) microgrid operation. More

specifically, our methodology is applied to a *medium voltage microgrid*, i.e., a power distribution network with distributed generation and energy storage, which network has the capability for grid-connected and standalone operation. Hourly load, wind and solar data are considered, because they have been already proved to be a very realistic representation for the case of ODGP [2]. In order for the microgrid to function optimally, it has to incorporate two types of DG units: (1) dispatchable (biomass in this paper), and (2) non-dispatchable (wind turbines and photovoltaics in this paper). The reason is that the output power of the dispatchable DGs can be easily regulated by special mechanisms, whereas the output power of the non-dispatchable DGs depends on stochastic variables, such as wind speed or solar irradiance, which means that non-dispatchable DGs carry a high degree of uncertainty. In the proposed formulation, energy storage systems (battery storage in this paper) have been integrated, as they are necessary, especially for the case of a standalone microgrid, where the power imbalances cannot be balanced by a main grid. Energy storage systems offer the ability to store the extra energy produced by the DG units when it is higher than the load demand and to discharge this energy when the DG units do not produce enough for the demand to be covered [4]. For energy storage systems, the planning of charge/discharge hours and the hourly planning of charge/discharge power is essential for the optimal functioning of the microgrid. The simultaneous capacity optimization of distributed generation and battery storage is formulated as a nonlinear optimization problem that is solved by sequential quadratic programming. The results prove the positive effect of the proposed optimal simultaneous capacity optimization of battery storage and distributed generation in the cases of grid-connected and standalone microgrid operation.

The article is structured as follows. Section 'Modelling of load, wind, and solar data' presents the modelling of load, wind, and solar data. Section 'Distributed generation and battery modelling' describes the modelling of DG and storage units. Section 'Problem formulation and solution' presents the proposed formulation and solution method for the simultaneous capacity optimization of battery storage and distributed generation for the cases of grid-connected and standalone microgrid. The data for a test case microgrid are given in Section 'Data for the test case microgrid'. Results and discussion for the cases of grid-connected and standalone microgrid operation are provided in Sections 'Results and discussion for the case of grid-connected microgrid' and 'Results and discussion for the case of standalone microgrid', respectively. Section 'Conclusion' concludes the paper.

## Modelling of load, wind, and solar data

The annual wind, solar, and ambient temperature data needed for the estimation of wind turbines and photovoltaics performance refer to measurements for the mountainous region of Keramia (altitude 500 m), in Chania, Crete, Greece [5]. These measurements were taken for a period of four years, and statistical analysis (e.g., peak, average, and minimum values) of the measurements was done. The annual peak load of the microgrid has been considered equal to 1.806 MW, whereas the necessary microgrid load profile was computed by downscaling the actual annual load profile of Crete [5]. In this paper, after retrieving this data, the annual wind speed, solar irradiance and load profile are utilized to generate, for each season (winter, spring, summer, fall), three representative typical days/states: one where each data element (wind speed, solar irradiance, and load) is at its maximum value, one where each data element is at its minimum value and one where each data element is as close as possible to its average value. More specifically, the average day of each season is the day for which its 24 hourly values present the lowest standard deviation compared to the corresponding 24 hourly average values of that season. Thus, there are in total 12 typical states throughout the year, each representing a certain amount of days and each consisting of 24 hourly time segments. This means that the actual states on which the problem works are 288. Thus, although the three data elements (wind speed, solar irradiance, and load) have a different probability distribution, the assumption of only 12 typical states is made to simplify the problem and facilitate the running of the software. Similar simplified assumptions are commonly used for the sizing of distributed generation and energy storage [2,20].

Each of these states is characterized by a possibility of occurrence (parameter $Poss_j$). More specifically, it is assumed that every typical day of every season has a certain probability to occur, which means that, e.g. in the winter, the probability of occurrence for the "maximum day" is $Poss_1$, the probability of occurrence for the "minimum day" is $Poss_2$, and the probability of occurrence for the "average day" is $Poss_3$, with $Poss_1 + Poss_2 + Poss_3 = 1$. For each hour of each state, three basic parameter values are calculated: the output of the wind turbines as a percentage of their rated power, the output of the photovoltaics as a percentage of their rated power and the load level as a percentage of its maximum. These parameter values ($wind_{j,t}$, $solar_{j,t}$ and $load_{j,t}$, respectively) are calculated in Section 'Distributed generation and battery modelling' and are integrated in the mathematical formulation of Section 'Problem formulation and solution'. The time-varying multilevel modelling of load, wind speed and solar irradiance data adopted in this paper has been already proved to be a very realistic representation for the case of ODGP [2,21,22]. In brief, this paper adopts the probabilistic methodology of [21] and [22], according to which a probabilistic load and generation model is created that combines the operating conditions of load levels and DG units using their respective probabilities, thus accommodating this model in a deterministic one.

## Distributed generation and battery modelling

### *Wind turbines modelling*

The power generated by the wind turbine (WT) is computed as follows [21]:

$$P_{w,out} = \begin{cases} 0, & \text{if } v_w < v_{ci} \\ P_{w,r} \cdot \frac{v_w - v_{ci}}{v_{w,r} - v_{ci}}, & \text{if } v_{ci} \leqslant v_w < v_{w,r} \\ P_{w,r}, & \text{if } v_{w,r} \leqslant v_w < v_{co} \\ 0, & \text{if } v_{co} \leqslant v_w \end{cases} \quad (1)$$

where $v_w$ is the wind speed, $v_{ci}$ is the cut-in wind speed, $v_{w,r}$ is the rated wind speed, $v_{co}$ is the cut-out wind speed, $P_{w,out}$ is the turbine output power, and $P_{w,r}$ is the turbine rated power. Eq. (1), which is the characteristic power curve of the wind turbine, shows that the output power is zero when the wind speed is too low or too high, linear when the wind speed varies between the cut-in and the rated wind speed, and equal to the rated power for wind speeds between the rated and the cut-out wind speed.

Thus, the ratio $P_{w,out}/P_{w,r}$ (parameter $wind_{j,t}$) is calculated from the wind speed data of each hour of each state. This parameter represents the output power of all the wind turbines at all buses, as a percentage of their rated power, during each hour of each state [21]. Thus, it is a global, only time-depending parameter that affects equally all wind turbines. The rated power at each bus is one of the design variables of the problem and is combined with parameter $wind_{j,t}$ in the power flow equations, to represent the actual power output (Section 'Power flow equations').

*Photovoltaics modelling*

The output power of the photovoltaics (PV) depends on the characteristics of the solar cell itself, as well as on the external irradiance and temperature conditions, according to the following equations [21]:

$$T_c = T_a + \frac{(T_n - 20)}{0.8} G \tag{2}$$

$$V = V_{oc} - K_v(T_c - 25) \tag{3}$$

$$I = G \cdot [I_{sc} + K_i(T_c - 25)] \tag{4}$$

$$FF = \frac{V_{\max} I_{\max}}{V_{oc} I_{sc}} \tag{5}$$

$$P_{s,out} = FF \cdot V \cdot I \tag{6}$$

where $T_a$ is the ambient temperature of the site, $T_n$ is the nominal operating temperature of the PV cell, $T_c$ is the temperature of the PV cell, $K_v$ is the voltage temperature coefficient, $K_i$ is the current temperature coefficient, $V_{oc}$ is the open circuit voltage, $I_{sc}$ is the short circuit current, $V_{\max}$ is the voltage at maximum power point, $I_{\max}$ is the current at maximum power point, $FF$ is the fill factor, $V$ is the voltage, $I$ is the current, $G$ is the solar irradiance, $P_{s,out}$ is the solar cell output power, and $P_{s,r}$ is the solar cell rated power.

The above equations describe the electrical behaviour of the PV cells. The more solar irradiance reaches the cell, the more current flows through it (Eq. (4)), resulting in higher output power (Eq. (6)). That is why in modern technologies the PV panels are tilted to face the sun directly, so as to gather maximum irradiance. Most of the parameters are given by the solar cells manufacturer.

Thus, the ratio $P_{s,out}/P_{s,r}$ (parameter $solar_{j,t}$) is calculated from the solar irradiance data of each hour of each state. This parameter represents the output power of all the photovoltaics at all buses, as a percentage of their rated power, during each hour of each state [21]. Thus, it is a global, only time-depending parameter that affects equally all photovoltaics. The rated power at each bus is one of the design variables of the problem and is combined with parameter $solar_{j,t}$ in the power flow equations, to represent the actual power output (Section 'Power flow equations'). The PVs are equipped with reactive power capable PV inverters [23].

*Biomass modelling*

The biomass unit is a dispatchable DG, so its output power is controllable on a daily basis. Its technology is considered to be gas turbine with biogas fuel. This type presents desirable operational characteristics, including wide range of operation, quick response, and ability for several starts and stops of operation per day. The cost curve of each biomass unit is assumed to be linear, whereas its rated power at a certain bus is considered equal to the maximum output power of this unit throughout the year. As a dispatchable DG, the operation of the biomass unit is not affected by external weather conditions, so there is no weather depending parameter, as in Sections 'Wind turbines modelling' and 'Photovoltaics modelling'.

*Battery modelling*

The battery storage system (BSS) consists mainly of a power conditioning system (PCS) and a storage unit. A PCS permits a BSS to generate both active and reactive power in all four quadrants [24]. The batteries that are used in this paper follow a daily charge–discharge cycle. Ideally, the daily energy stored should be fully released. Due to energy losses, though, the battery efficiency drops. In this model, the batteries charge power during some hours and discharge power to the microgrid during other hours. Thus, they can be modelled either as a load or as a power source. The exact charge–discharge hours can be easily regulated, taking into consideration the hourly load and climate conditions. The following equations are used [17]:

$$Ech_{j,i} = \sum_{t=1}^{24} Pch_{j,t,i} \quad \forall\, j,i \tag{7}$$

$$Edis_{j,i} = \sum_{t=1}^{24} Pdis_{j,t,i} \quad \forall\, j,i \tag{8}$$

$$Pch_{j,t,i} \leqslant P_i \quad \forall\, j,t,i \tag{9a}$$

$$Pdis_{j,t,i} \leqslant P_i \quad \forall\, j,t,i \tag{9b}$$

$$Ech_{j,i} \leqslant E_i \quad \forall j,\ i \tag{10}$$

Eq. (7) (Eq. (8)) shows that the total energy charged (discharged) at the battery of each bus, during each state, is equal to the daily sum of the energy charged (discharged) at each hour. This hourly energy is arithmetically equal to the hourly power the battery charges or discharges, as the latter is constant and the time segment is 1 h. Eqs. (9a) and (9b) indicate that the active power capacity is equal or higher than the maximum hourly power charged or discharged throughout the year. Eq. (10) shows that the energy storage capacity is equal or higher than the maximum daily energy charged throughout the year.

## Problem formulation and solution

This section presents the proposed formulation of the simultaneous capacity optimization of storage and distributed generation in a microgrid that operates either grid-connected or standalone. The proposed formulation constitutes a nonlinear programming optimization problem that seeks the optimum sizes of distributed resources (WT, PV, biomass, and battery) to be installed into an existing microgrid, so as to either minimize the total annual energy loss of the microgrid or to minimize the cost of energy, subject to microgrid network operating constraints and battery operation constraints. It should be noted that the considered distributed resources (WT, PV, biomass, and battery) can be placed at selected buses of the microgrid, which are called feasible connection points [25]. As a result, the proposed formulation aims at finding which types of distributed resources are really needed at each specific bus, together with the sizes of the distributed resources.

*Objective functions*

In this paper, two alternative objective functions are investigated:

1. The minimization of the total annual energy loss (*TAEL*), defined in Section 'Minimizing TAEL'.
2. The minimization of the cost of energy (*COE*), defined in Section 'Minimizing COE'.

*Minimizing TAEL*

In this case, the objective function is the minimization of the total annual energy loss (*TAEL*) due to the resistance of the lines. Alternatively, the minimization of the total power loss of the system, which is another objective often used in ODGP [2], could be also considered. The *TAEL* objective, which is commonly used in DG planning problems [2,21,22,26], is computed as follows [21]:

$$TAEL = \sum_{j=1}^{12} Days_j \cdot Poss_j \cdot \sum_{t=1}^{24} Powerloss_{j,t} \quad (11)$$

where

$$Powerloss_{j,t} = 0.5 \sum_{i,k} G_{ik} \left[ v_{j,t,i}^2 + v_{j,t,k}^2 - 2 v_{j,t,i} v_{j,t,k} \cos(\delta_{j,t,k} - \delta_{j,t,i}) \right] \quad \forall j,t \quad (12)$$

The total power loss at each hour of each state, $Powerloss_{j,t}$, is obtained from the usual power flow equations. It should be noted that Eq. (12) refers to pairs of different buses, so the sum is valid only for different values of $i$ and $k$, thus $i \neq k$. The factor 0.5 is put because each bus combination appears twice in the sum. This hourly power loss is arithmetically equal to the hourly energy loss of the lines, as the power is constant and the time segment is one hour. This energy loss is then summed up for all the hours and days of the year to give the total annual energy loss (Eq. (11)). There are 3 possible typical days/states in each of the 4 seasons. Each of these 3 states is associated with a possibility of occurrence, which is represented by parameter $Poss_j$. For each season, these possibilities sum up to 1, so Eq. (11) is, in fact, a sum with different weights on the daily energy loss of each possible state.

*Minimizing COE*

In this case, the objective function is the minimization of the cost of energy (*COE*) [5]. The cost of energy is a very good measure of power generation cost; that is why *COE* is commonly used in sizing distributed energy resources [27]. The cost of energy is computed as follows [5,27]:

$$COE = \frac{C_{antot}}{E_{anserved}} \quad (13a)$$

where

$$\begin{aligned} C_{antot} = & C_{exch} \cdot \sum_{j=1}^{12} Days_j \cdot Poss_j \cdot \sum_{t=1}^{24} Pin_{j,t,1} + CRF \cdot \sum_i (CI_w \cdot Pw_i \\ & + CI_s \cdot Ps_i + CI_b \cdot \max_j(Pb_{j,i}) + CI_e \cdot P_i) \\ & + \sum_i (CM_w \cdot Pw_i + CM_s \cdot Ps_i + CM_b \cdot \max_j(Pb_{j,i}) + CM_e \cdot P_i) \\ & + \sum_{t=1}^{24} \sum_{j=1}^{12} Days_j \cdot Poss_j \cdot \sum_i (Bio_a + Bio_b \cdot Pb_{j,i}) \end{aligned} \quad (13b)$$

$$\begin{aligned} E_{anserved} = & \sum_{j=1}^{12} Days_j \cdot Poss_j \cdot \sum_{t=1}^{24} Psold_{j,t,1} + \sum_i \sum_{j=1}^{12} Days_j \cdot Poss_j \\ & \cdot \sum_{t=1}^{24} load_{j,t} \cdot P_{bus\ i} \end{aligned} \quad (13c)$$

Eq. (13a) shows that the *COE* is equal to the ratio of the total annualized cost ($C_{antot}$) to the total annual energy served ($E_{anserved}$). More specifically, Eq. (13b) indicates that the total annualized cost consists of the cost the microgrid pays or is paid when energy is bought (positive $Pin_{j,t,1}$) or sold (negative $Pin_{j,t,1}$) through the substation, the annualized capital (investment) costs for DGs and batteries, the annualized maintenance costs for DGs and batteries, and the annual biomass fuel cost, which is only calculated for the scenarios that include biomass units. Eq. (13c) shows that the total annual energy served is the sum of the hourly energy that is sold to the main grid (when this happens) plus the total load served throughout the year.

*Constraints of grid-connected microgrid*

The constraints involve technical constraints of the microgrid, as well as battery daily cycle constraints.

*Power flow equations*

$$\begin{aligned} & Pin_{j,t,1} + wind_{j,t} Pw_i + solar_{j,t} Ps_i + Pb_{j,i} - Pch_{j,t,i} + Pdis_{j,t,i} - load_{j,t} P_{bus\ i} \\ & = v_{j,t,i}^2 G_{ii} + v_{j,t,i} \sum_k v_{j,t,k} (G_{ik} \cos(\delta_{j,t,i} - \delta_{j,t,k}) + B_{ik} \sin(\delta_{j,t,i} - \delta_{j,t,k})), \forall j,t,i \end{aligned} \quad (14)$$

$$\begin{aligned} & Qin_{j,t,1} + \tan\phi_w wind_{j,t} Pw_i + \tan\phi_s solar_{j,t} Ps_i + \tan\phi_b Pb_{j,i} - Qch_{j,t,i} \\ & + Qdis_{j,t,i} - load_{j,t} Q_{bus\ i} = -v_{j,t,i}^2 B_{ii} + v_{j,t,i} \sum_k v_{j,t,k} (G_{ik} \sin(\delta_{j,t,i} - \delta_{j,t,k}) \\ & - B_{ik} \cos(\delta_{j,t,i} - \delta_{j,t,k})), \quad \forall j,t,i \end{aligned} \quad (15)$$

The above equations show that the active or reactive power injected at each bus comes from the DG sources and the discharging of the batteries, whereas at each bus, power is absorbed from the loads as well as the charging of the batteries. The terms $Pin_{j,t,1}$ and $Qin_{j,t,1}$ are used only for the slack bus ($i = 1$) and refer to the power exchange between the main grid and the microgrid through the substation. Positive values mean that power is injected in the microgrid from the main grid, whereas negative values mean that power is injected in the main grid from the microgrid. Thus, the substation plays a crucial role, balancing the power flow of the system. As in Eq. (12), the sums are valid for $i \neq k$.

*Voltage limits at all buses*

$$v_{\min} \leqslant v_{j,t,i} \leqslant v_{\max} \quad \forall j,t,i \quad (16)$$

$$\delta_{\min} \leqslant \delta_{j,t,i} \leqslant \delta_{\max} \quad \forall j,t,i \quad (17)$$

*Voltage at slack bus (considered to be bus 1)*

$$v_{j,t,1} = 1\ p.u. \quad \forall j,t \quad (18)$$

$$\delta_{j,t,1} = 0 \quad \forall j,t \quad (19)$$

*Demand covering*

The total power discharged by the batteries at any hour should be no more than the total demand during that hour, in order to

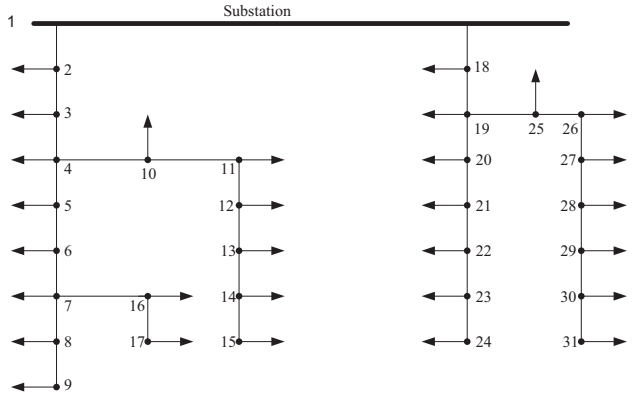


**Fig. 1.** 31-bus medium voltage microgrid.

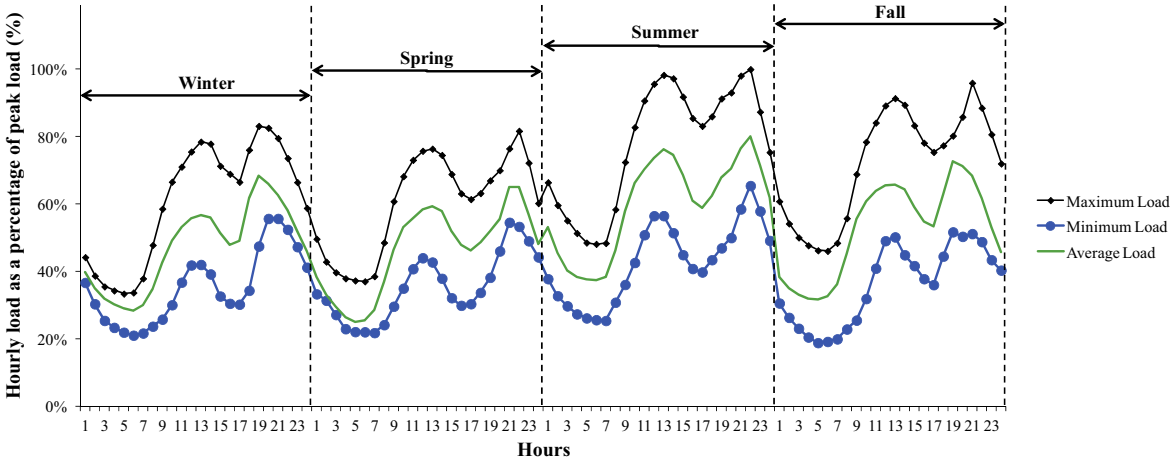


**Fig. 2.** Hourly load, for all the seasons, at all buses, as a percentage of peak load.

minimize the power exchange between the microgrid and the main network [17]:

$$\sum_i (Pdis_{j,t,i}) \leqslant \sum_i load_{j,t} P_{bus\ i} \quad \forall j,t \tag{20}$$

*Daily battery cycle*

In order to facilitate the system operation, the following practical rule is applied: the daily energy discharged by the batteries should be equal to the daily energy charged multiplied by the battery efficiency, so that no energy is accumulated day after day.

$$Edis_{j,i} = eff \cdot Ech_{j,i} \quad \forall j,i \tag{21}$$

$$Qch_{j,t,i} = \tan\phi_e \cdot Pch_{j,t,i} \quad \forall j,t,i \tag{22}$$

$$Qdis_{j,t,i} = \tan\phi_e \cdot Pdis_{j,t,i} \quad \forall j,t,i \tag{23}$$

*Auxiliary variables for substation power*

Through the substation, power can be: (1) injected (positive $Pin_{j,t,1}$), i.e., $Pbought_{j,t,1}$ is the power the microgrid buys from the transmission network, or (2) absorbed (negative $Pin_{j,t,1}$), i.e., $Psold_{j,t,1}$ is the power the microgrid sells to the transmission network. This separation is necessary in order to calculate the first term of Eq. (13c). Consequently, the auxiliary variables $Pbought_{j,t,1}$ and $Psold_{j,t,1}$ are computed as follows:

$$Pbought_{j,t,1} = \begin{cases} Pin_{j,t,1}, & \text{if } Pin_{j,t,1} > 0 \\ 0, & \text{if } Pin_{j,t,1} \leqslant 0 \end{cases} \quad \forall j,t \tag{24}$$

$$Psold_{j,t,1} = \begin{cases} 0, & \text{if } Pin_{j,t,1} \geqslant 0 \\ -Pin_{j,t,1}, & \text{if } Pin_{j,t,1} < 0 \end{cases} \quad \forall j,t \tag{25}$$

This is modeled in GAMS as follows:

$$Pin_{j,t,1} = Pbought_{j,t,1} - Psold_{j,t,1} \quad \forall j,t \tag{26}$$

where

$$Pbought_{j,t,1} \geqslant 0 \quad \forall j,t \tag{27}$$

$$Psold_{j,t,1} \geqslant 0 \quad \forall j,t \tag{28}$$

$$Pbought_{j,t,1} \cdot Psold_{j,t,1} = 0 \quad \forall j,t \tag{29}$$

Eq. (29) means that at least one of the two parameters ($Pbought_{j,t,1}$ and $Psold_{j,t,1}$) is always zero, so, taking also Eq. (26) into account, $Pin_{j,t,1}$ is always equal to only one of these two parameters ($Pbought_{j,t,1}$ or $-Psold_{j,t,1}$).

*Extra constraints for standalone microgrid*

The constraints (30) and (31) are applicable only for the standalone operation of the microgrid, when the real and reactive power that is exchanged through the substation should be as low as possible, which is controlled with the use of the control parameter $a$, which has to take very low value, e.g., $a = 0.002$. This parameter, multiplied with the sum of the rated load at all buses, sets the strict boundaries for the power exchange, forcing the microgrid to function, in fact, autonomously:

$$-a \cdot P_{load,total} \leqslant Pin_{j,t,1} \leqslant a \cdot P_{load,total} \quad \forall j,t \tag{30}$$

$$-a \cdot Q_{load,total} \leqslant Qin_{j,t,1} \leqslant a \cdot Q_{load,total} \quad \forall j,t \tag{31}$$

*Design variables and solution method*

The design variables of the optimization problem (11)–(31) are the following:

1. At each bus $i$, the capacity size (MW) of the DG units is the first group of design variables. More specifically, these design variables are the rated wind power ($Pw_i$), the rated solar power ($Ps_i$), and the rated biomass power ($\max_j(Pb_{j,i})$).
2. At each bus $i$, the capacity size (MW) of the batteries, which is denoted by the variable $P_i$, is the second group of design variables.
3. At each bus $i$, the energy size (MW h) of the batteries, which is denoted by the variable $E_i$, is the third group of design variables.

The optimization problem (11)–(31) is a nonlinear programming problem that is solved by a sequential quadratic programming algorithm on General Algebraic Modelling System (GAMS) environment, using the SNOPT solver of GAMS [28]. Sequential quadratic programming was chosen, since it is one of the best methods for solving nonlinear programming problems [29], [30].

The batteries can either charge from the power produced by the DGs or from the power that origins from the main grid through the substation. There is no power flow limitation as to where the charge power comes from. It is up to the solver to determine the exact power flow in the microgrid at each hour of each state, so as to optimize the objective function.

**Table 1**
Results for grid-connected microgrid, minimizing TAEL, examining all studied scenarios.

| Candidate buses | Scenarios | | | | | | | | | | | |
|---|---|---|---|---|---|---|---|---|---|---|---|---|
| | Initial system, no DGs | Only wind power | Only solar power | Only biomass power | All 3 DG types | | | All DG types and batteries | | | | |
| | | Wind turbines rated power (MW) | PVs rated power (MW) | Biomass units rated power (MW) | Wind turbines rated power (MW) | PVs rated power (MW) | Biomass units rated power (MW) | Wind turbines rated power (MW) | PVs rated power (MW) | Biomass units rated power (MW) | Batteries rated power (MW) | Batteries energy rating (MW h) |
| Bus 2 | – | 0 | 0.826 | 0 | 0 | 0.162 | 0 | 0 | 0.399 | 0 | 0.299 | 1.528 |
| Bus 4 | – | 0.398 | 0 | 0 | 0.096 | 0 | 0 | 0.129 | 0 | 0 | 0.179 | 0.972 |
| Bus 6 | – | 0 | 0.350 | 0 | 0 | 0.065 | 0 | 0 | 0.345 | 0 | 0.297 | 1.832 |
| Bus 7 | – | 0.210 | 0 | 0 | 0.037 | 0 | 0 | 0.041 | 0 | 0 | 0.142 | 0.530 |
| Bus 10 | – | 0 | 0 | 0.764 | 0 | 0 | 0.455 | 0 | 0 | 0.196 | 0 | 0 |
| Bus 11 | – | 0 | 0.374 | 0 | 0 | 0.037 | 0 | 0 | 0.348 | 0 | 0.333 | 2.047 |
| Bus 13 | – | 0.232 | 0 | 0 | 0.162 | 0 | 0 | 0.156 | 0 | 0 | 0.130 | 0.718 |
| Bus 17 | – | 0 | 0 | 0.191 | 0 | 0 | 0.216 | 0 | 0 | 0.457 | 0 | 0 |
| Bus 18 | – | 0.532 | 0 | 0 | 0 | 0 | 0 | 0 | 0 | 0 | 0.166 | 0.801 |
| Bus 19 | – | 0 | 0 | 0.921 | 0 | 0 | 0.738 | 0 | 0 | 0.735 | 0 | 0 |
| Bus 22 | – | 0 | 0.362 | 0 | 0 | 0 | 0 | 0 | 0.133 | 0 | 0.087 | 0.393 |
| Bus 24 | – | 0 | 0 | 0.286 | 0 | 0 | 0.351 | 0 | 0 | 0.093 | 0 | 0 |
| Bus 28 | – | 0 | 0.752 | 0 | 0 | 0.328 | 0 | 0 | 1.322 | 0 | 1.098 | 7.107 |
| Bus 30 | – | 0.548 | 0 | 0 | 0.371 | 0 | 0 | 0.192 | 0 | 0 | 0.411 | 2.425 |
| Total rated power or energy | – | **1.920** | **2.664** | **2.162** | **0.666** | **0.592** | **1.760** | **0.518** | **2.547** | **1.481** | **3.142** | **18.353** |
| Annual energy loss (MW h), objective function | **199.360** | **101.984** | **123.367** | **86.372** | **43.754** | | | **17.082** | | | | |
| Loss reduction in comparison with the initial system (%) | 0 | 49 | 38 | 57 | 78 | | | 91 | | | | |
| COE (€/MW h) | **51.213** | **54.404** | **51.939** | **169.808** | **174.793** | | | **206.255** | | | | |

**Table 2**
Results for grid-connected microgrid, minimizing COE, examining all studied scenarios.

| Candidate buses | Scenarios | | | | | | | | | | | |
|---|---|---|---|---|---|---|---|---|---|---|---|---|
| | Initial system, no DGs | Only wind power | Only solar power | Only biomass power | All 3 DG types | | | All DG types and batteries | | | | |
| | | Wind turbines rated power (MW) | PVs rated power (MW) | Biomass units rated power (MW) | Wind turbines rated power (MW) | PVs rated power (MW) | Biomass units rated power (MW) | Wind turbines rated power (MW) | PVs rated power (MW) | Biomass units rated power (MW) | Batteries rated power (MW) | Batteries energy rating (MW h) |
| Bus 2 | – | 0 | 0.991 | 0 | 0 | 0.197 | 0 | 0 | 0.609 | 0 | 0 | 0 |
| Bus 4 | – | 0.808 | 0 | 0 | 2.015 | 0 | 0 | 0 | 0 | 0 | 0 | 0 |
| Bus 6 | – | 0 | 0.319 | 0 | 0 | 0 | 0 | 0 | 0 | 0 | 0 | 0 |
| Bus 7 | – | 0.178 | 0 | 0 | 0.077 | 0 | 0 | 0 | 0 | 0 | 0 | 0 |
| Bus 10 | – | 0 | 0 | 0 | 0 | 0 | 0 | 0 | 0 | 1.564 | 0 | 0 |
| Bus 11 | – | 0 | 0.338 | 0 | 0 | 0 | 0 | 0 | 0 | 0 | 0.087 | 0.420 |
| Bus 13 | – | 0.182 | 0 | 0 | 0.083 | 0 | 0 | 0 | 0 | 0 | 0.119 | 0.789 |
| Bus 17 | – | 0 | 0 | 0.694 | 0 | 0 | 0 | 0 | 0 | 0 | 0 | 0 |
| Bus 18 | – | 1.841 | 0 | 0 | 0.296 | 0 | 0 | 0.092 | 0 | 0 | 0 | 0 |
| Bus 19 | – | 0 | 0 | 3.801 | 0 | 0 | 3.762 | 0 | 0 | 3.932 | 0 | 0 |
| Bus 22 | – | 0 | 0.349 | 0 | 0 | 0 | 0 | 0 | 0 | 0 | 0 | 0 |
| Bus 24 | – | 0 | 0 | 0 | 0 | 0 | 0 | 0 | 0 | 0.930 | 0 | 0 |
| Bus 28 | – | 0 | 0.674 | 0 | 0 | 0.230 | 0 | 0 | 0.040 | 0 | 0.049 | 0.116 |
| Bus 30 | – | 0.460 | 0 | 0 | 0 | 0 | 0 | 0.162 | 0 | 0 | 0.130 | 0.732 |
| Total rated power or energy | – | **3.469** | **2.671** | **4.495** | **2.471** | **0.427** | **3.762** | **0.254** | **0.649** | **6.426** | **0.385** | **2.057** |
| Annual energy loss (MW h) | **199.360** | **140.717** | **124.039** | **930.178** | **792.927** | | | **1700.563** | | | | |
| COE (€/MW h), objective function | **51.213** | **48.032** | **51.909** | **42.372** | **38.065** | | | **23.853** | | | | |
| Cost reduction in comparison with the initial system (%) | 0 | 6 | −1 | 17 | 26 | | | 53 | | | | |

## Data for the test case microgrid

The system under study consists of a 31-bus medium voltage (MV) microgrid (Fig. 1), which is part of the 69-bus radial distribution feeder, the data of which can be found in [31]. The MV level is 11 kV, with limits of ±6% for the voltage magnitude [31] at all buses except the slack bus for which the voltage magnitude is kept at its nominal value according to constraint (18). Fig. 2 presents the load at all buses as a percentage of their peak load (parameter $load_{j,t}$) for all the hours of each state of each season.

The wind speed, solar irradiance and load data are taken from measurements for the island of Crete, Greece (Section 'Modelling of load, wind, and solar data'). The wind turbines used have a cut-in wind speed of 4 m/s, a rated wind speed of 16 m/s and a cut-out speed of 25 m/s [21]. Their power factor is assumed to be 0.9 lagging. They can be connected at buses 4, 7, 13, 18 and 30. The power factor of the photovoltaics is assumed to be 0.8 lagging. The photovoltaics can be connected at buses 2, 6, 11, 22, 28. Biomass units have a maximum efficiency of 36%, whereas their power factor is assumed to be 0.8 lagging. They can be connected at buses 10, 17, 19, 24.

The batteries follow two different daily cycles: (1) *Type A batteries* charging from 8:00 until 20:00 (hours 9–20) and discharging from 20:00 until 8:00 (hours 1–8 and 21–24), whose candidate buses are 2, 6, 11, 22 and 28, and (2) *Type B batteries* discharging from 8:00 until 20:00 and charging from 20:00 until 8:00 (reverse cycle in comparison with Type A batteries), whose candidate buses are 4, 7, 13, 18 and 30. More specifically, Type A batteries take advantage of the high solar irradiance during the day (as they are connected at the same buses that also have photovoltaics connected), thus storing energy, which they can release during the night. Type B batteries, on the other hand, take advantage of the wind speed during the night (as they are connected at the same buses that also have wind turbines connected), in combination with the low load demand during these hours, thus storing energy, which they can release during the day, when the load demand is high. These two types are thus complementary, so at every hour, energy can be stored and released simultaneously in the microgrid. The battery efficiency is 75% and the ESS power factor is assumed to be 0.8 lagging, which means that ESS charges or discharges both real and reactive power.

It should be noted that the concept of establishing in advance in which time steps the batteries charge and discharge has been successfully applied in [17] for the optimal sizing of batteries in

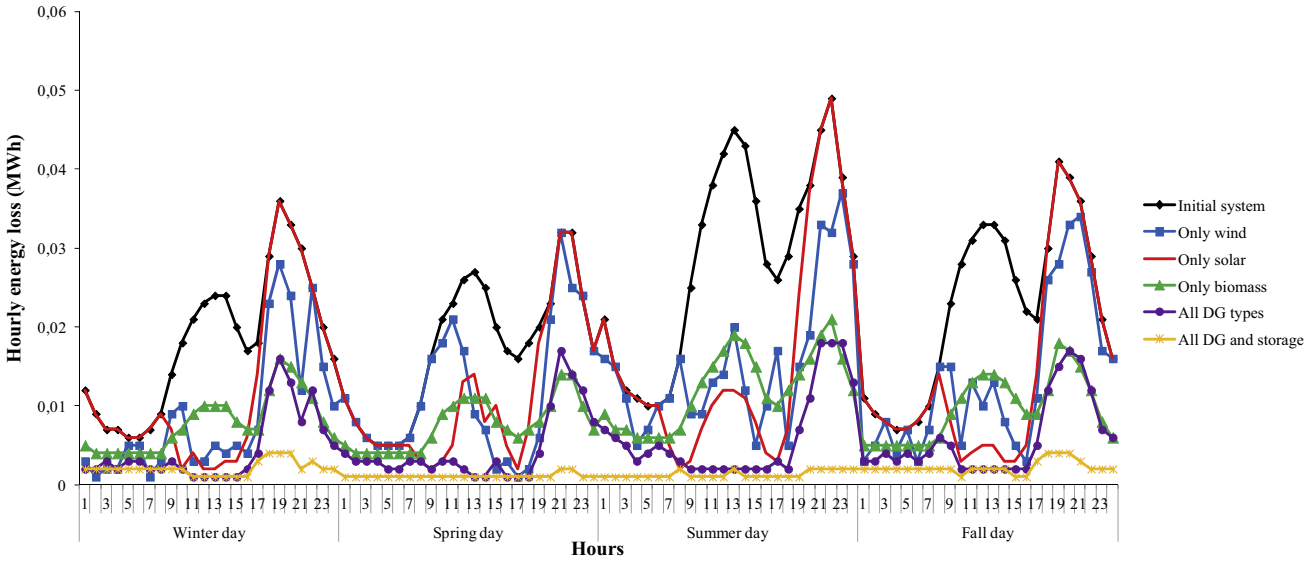


**Fig. 3.** Hourly energy loss (MW h) for the average day of each season, for all the examined scenarios of the grid-connected microgrid, when minimizing TAEL.

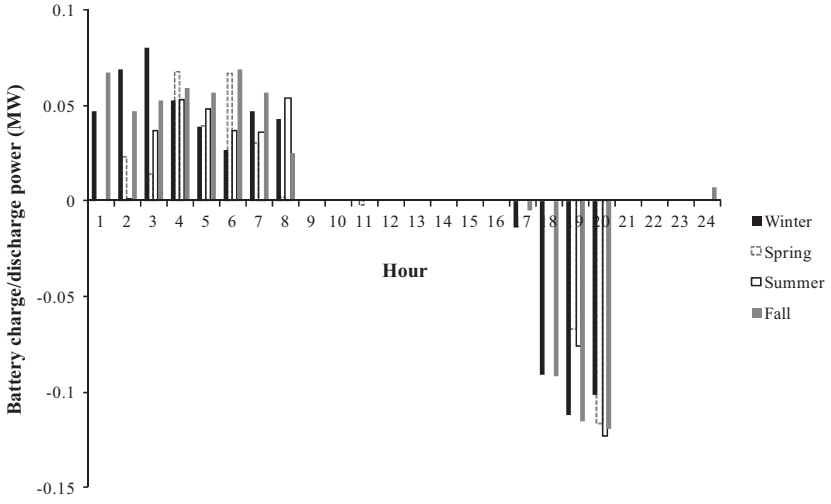


**Fig. 4.** Hourly charge power (positive values)/discharge power (negative values), in MW, for the average day of each season, for the battery connected at bus 4, in grid-connected operation, when minimizing TAEL.

distribution systems with a high wind energy penetration, where one type of batteries charging/discharging profile is used, while in this paper, two types of batteries charging/discharging profiles are used. Interested readers can find more information in [32] regarding the optimal selection of charging/discharging scheduling of batteries in distribution systems with PV generation systems.

As is common practice for the analyzed case study system, a fixed price (parameter $C_{exch}$) of 50 €/MW h is considered for the energy bought from the main grid or sold to it through the substation. However, in other case study networks, an energy tariff could be also used.

## Results and discussion for the case of grid-connected microgrid

In the case of a grid-connected operation, i.e., the microgrid of Section 'Data for the test case microgrid' is connected to the main grid through the substation, various scenarios are tested and the results shown in Tables 1 and 2 are discussed in Sections 'Minimizing TAEL' and 'Minimizing COE', respectively. More specifically, Tables 1 and 2 present the rated power of the DGs and batteries and the energy rating of the batteries at each candidate bus, for all the scenarios studied. The total rated power is then calculated underneath. The value of the objective function is presented for all the scenarios, as well its reduction (in comparison with the initial microgrid that has neither DGs nor batteries). Finally, the value of the other objective function (which is just calculated from the results, by the software, and not minimized) is also shown.

### *Minimizing TAEL*

It can be seen from Table 1 that the installation of even one DG type reduces the microgrid annual energy losses by 38% for the case of PV, 49% for the case of WT and 57% for the case of biomass DG. The maximum annual energy loss reduction is achieved by the biomass DGs, since their production is constant and regulated. Examining the non-dispatchable units, the photovoltaics reduce the losses less than the wind turbines, because there is no irradiance at night, so during these hours there is no actual difference with the initial system, whereas the wind can blow at any time.

When all three DG types are installed (wind, solar, and biomass), the microgrid annual energy losses are reduced by 78%, since there is a kind of co-operation between the DG units.

In a microgrid containing all three types of DG units, the addition of battery storage units achieves the maximum annual energy loss reduction for the microgrid, namely 91%. In this case, the highest values for the battery rated power are observed at the buses that also contain photovoltaics. A high solar energy penetration in the system is also observed. On the other hand, the buses that also contain wind turbines have a lower battery rated power. Thus, the batteries operate with higher power when following a daily cycle of charging during the day and discharging during the night.

It can be observed from Table 1 that the cost of energy (which, in this case, is just calculated) constantly increases when installing more types of DG and storage units. This remark is very interesting; however it should not be taken for granted to happen in any other case, as it depends on the parameters of the test case microgrid (e.g., the values of the cost parameters involved in the calculation of COE).

The hourly energy loss at the average day of each season, for all the scenarios, is shown in Fig. 3. It can be observed that the maximum losses occur late in the evening, as it is then that the load levels are at their maximum. By installing storage units, though, the hourly variations are almost eliminated.

In Figs. 4 and 5, the daily battery cycles (at buses 4 and 28, respectively) for the average day of each season are presented. For night-charging batteries (bus 4), the whole energy is discharged in the evening (Fig. 4). For day-charging batteries (bus 28), the charging follows in some way the sun profile, as the peak occurs at noon hours, and the discharging is uniform at all hours (Fig. 5).

### *Minimizing COE*

In this case, it can be seen from Table 2 that the results are quite similar with the ones of Section 'Minimizing TAEL' concerning which DG types provide a better optimization. The biomass units are the most efficient in reducing the cost. In this case, the difference is that the total rated power of the DGs is mostly concentrated at the buses closest to the slack bus (Fig. 1). A possible explanation for this is that DG units at these buses provide more power directly to the main grid, resulting in more energy sold (Eq. (13c)), which also provides a lower cost (Eq. (13b)).

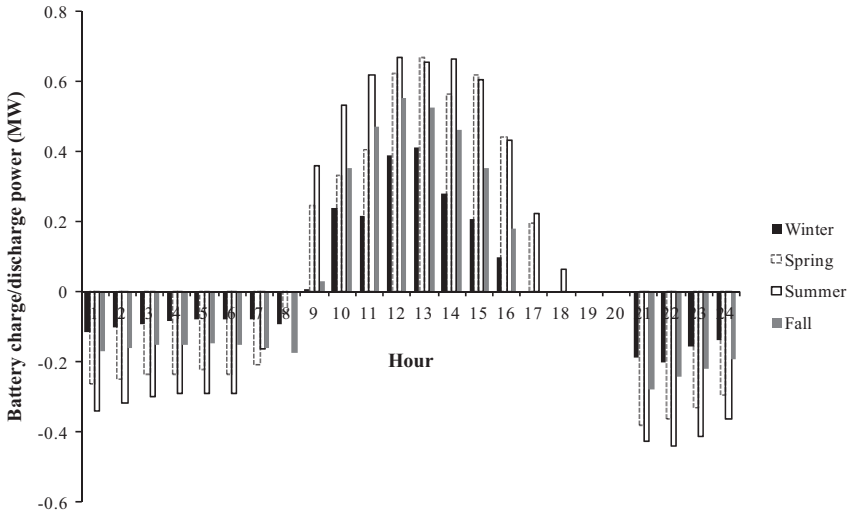


**Fig. 5.** Hourly charge power (positive values)/discharge power (negative values), in MW, for the average day of each season, for the battery connected at bus 28, in grid-connected operation, when minimizing TAEL.

It should be noted that the annual energy losses (which, in this case, are just calculated) do not drop by installing more DG types and batteries. In contrary, they increase significantly. This is due to the fact that priority is given to the cost and not to the power flow, since the optimization objective is the minimization of the cost of energy.

## Results and discussion for the case of standalone microgrid

In the case of standalone operation, the microgrid of Section 'Data for the test case microgrid' is disconnected from the main grid. The control parameter $a$ is set equal to 0.002. It should be noted that these very small power imbalances of 0.2% ($a = 0.002$) can be balanced as follows: the substation can be replaced, in reality, by a small DG plant when injecting power and by a dump load when absorbing power.

The results are shown in Tables 3 and 4. They present the rated power of the DGs and batteries and the energy rating of the batteries at each candidate bus, for standalone operation of the microgrid. The total rated power is then calculated underneath. The value of the objective function is also presented. Finally, the value of the other objective function (which is just calculated from the results, by the software, and not minimized) is also shown.

### *Minimizing TAEL*

The results for the standalone microgrid are shown in Table 3. In this case, the standalone microgrid annual energy losses are comparative to those of the grid-connected microgrid with neither DG nor storage units. The cost of energy is higher, too. Also, the rated power of non-dispatchable DG units is very low; these units are almost unnecessary. On the other hand, the biomass rated power, as well as the battery rated power and energy rating are highly increased. This means that the standalone microgrid needs these units much more than the grid-connected microgrid. In the case of standalone microgrid, the power imbalances cannot be balanced by the main grid anymore, so the biomass units and the batteries undertake this task. The conclusion is that the standalone operation of the microgrid necessitates more certain, well-programmed dispatchable units (biomass and battery), rather than non-dispatchable units (WT and PV) with uncertain and non-controllable output power.

In Fig. 6, the mean daily real power injected or absorbed through the substation for some of the examined cases is presented, when minimizing TAEL. It can be concluded that the DG and storage units make the microgrid much more autonomous, as it needs much less power exchange with the main grid.

**Table 3**
Results for standalone microgrid, minimizing TAEL.

| Candidate buses | Wind turbines rated power (MW) | PVs rated power (MW) | Biomass units rated power (MW) | Batteries rated power (MW) | Batteries energy rating (MW h) |
|---|---|---|---|---|---|
| Bus 2 | 0 | 0 | 0 | 1.485 | 3.950 |
| Bus 4 | 0 | 0 | 0 | 1.799 | 5.361 |
| Bus 6 | 0 | 0 | 0 | 1.625 | 5.566 |
| Bus 7 | 0 | 0 | 0 | 1.631 | 5.336 |
| Bus 10 | 0 | 0 | 0.824 | 0 | 0 |
| Bus 11 | 0 | 0 | 0 | 1.365 | 3.763 |
| Bus 13 | 0.174 | 0 | 0 | 0.687 | 2.272 |
| Bus 17 | 0 | 0 | 0.537 | 0 | 0 |
| Bus 18 | 0 | 0 | 0 | 1.495 | 9.709 |
| Bus 19 | 0 | 0 | 1.046 | 0 | 0 |
| Bus 22 | 0 | 0 | 0 | 1.094 | 3.502 |
| Bus 24 | 0 | 0 | 0.296 | 0 | 0 |
| Bus 28 | 0 | 0 | 0 | 0.816 | 4.187 |
| Bus 30 | 0.188 | 0 | 0 | 0.728 | 3.745 |
| Total rated power or energy | **0.362** | **0** | **2.703** | **12.725** | **47.391** |
| Annual energy loss (MW h), objective function | **189.153** | | | | |
| COE (€/MW h) | **235.447** | | | | |

**Table 4**
Results for standalone microgrid, minimizing COE.

| Candidate buses | Wind turbines rated power (MW) | PVs rated power (MW) | Biomass units rated power (MW) | Batteries rated power (MW) | Batteries energy rating (MW h) |
|---|---|---|---|---|---|
| Bus 2 | 0 | 0 | 0 | 0.798 | 2.913 |
| Bus 4 | 0 | 0 | 0 | 0 | 0 |
| Bus 6 | 0 | 0 | 0 | 0.532 | 2.095 |
| Bus 7 | 0.099 | 0 | 0 | 0.831 | 2.748 |
| Bus 10 | 0 | 0 | 0.581 | 0 | 0 |
| Bus 11 | 0 | 0 | 0 | 0.295 | 1.603 |
| Bus 13 | 0 | 0 | 0 | 0.664 | 1.873 |
| Bus 17 | 0 | 0 | 0.069 | 0 | 0 |
| Bus 18 | 0.001 | 0 | 0 | 0.802 | 2.597 |
| Bus 19 | 0 | 0 | 0.824 | 0 | 0 |
| Bus 22 | 0 | 0 | 0 | 0.693 | 2.848 |
| Bus 24 | 0 | 0 | 0.341 | 0 | 0 |
| Bus 28 | 0 | 0 | 0 | 0.181 | 0.973 |
| Bus 30 | 0.214 | 0 | 0 | 0.804 | 5.902 |
| Total rated power or energy | **0.314** | **0** | **1.815** | **5.600** | **23.552** |
| Annual energy loss (MW h) | **422.951** | | | | |
| COE (€/MW h), objective function | **151.054** | | | | |

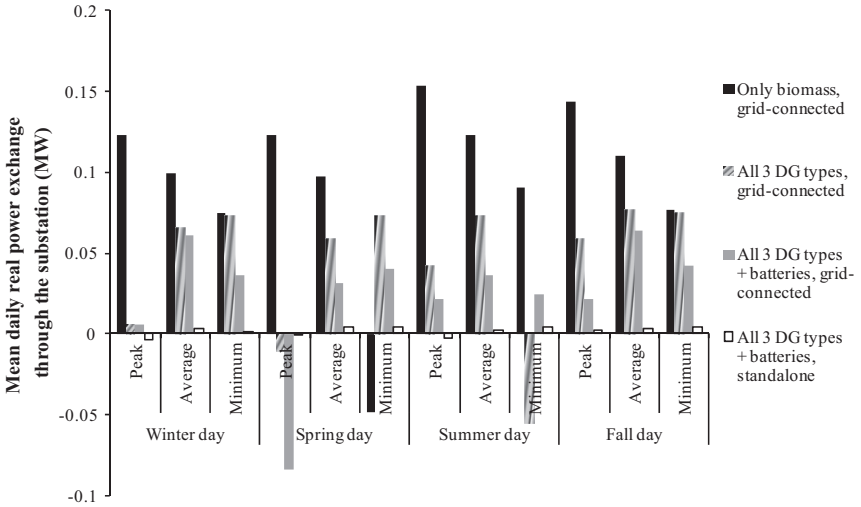


**Fig. 6.** Mean daily real power injected or absorbed through the substation for some of the examined cases, when minimizing TAEL.

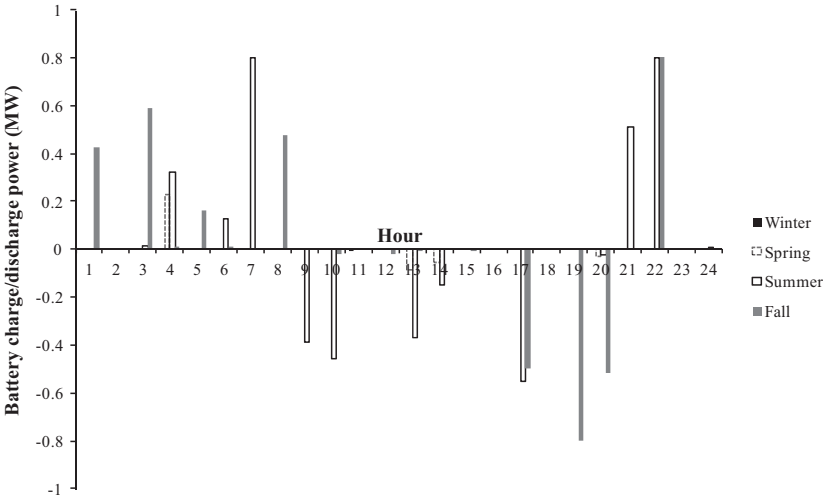


**Fig. 7.** Hourly charge power (positive values)/discharge power (negative values), in MW, for the average day of each season, for the battery connected at bus 18, in standalone operation, when minimizing COE.

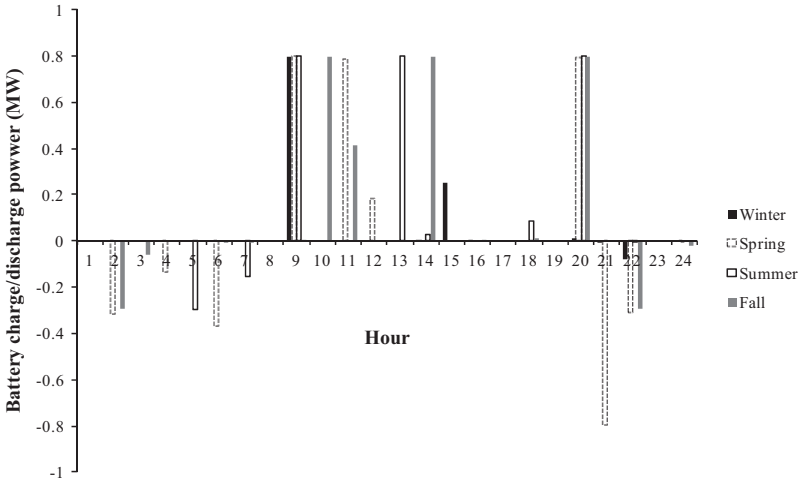


**Fig. 8.** Hourly charge power (positive values)/discharge power (negative values), in MW, for the average day of each season, for the battery connected at bus 2, in standalone operation, when minimizing COE.

*Minimizing COE*

In the case of standalone microgrid, it can be seen from Table 4 that the COE increases significantly, in comparison to the COE of the grid-connected microgrid (Table 2). This is reasonable and expected because, firstly, there is practically no energy sold (Eq. (30)) and, secondly, forcing the microgrid to function autonomously sets much more restrictions to the whole problem meaning that the total annual energy served has to be produced by the distributed energy resources of the microgrid. Also, the total DG rated power is very low, especially of the non-dispatchable units, whereas the battery power and energy rating are much higher. Less energy is produced, resulting in lower energy losses (Table 4). The importance of energy storage systems in standalone microgrids is thus proved again in this case.

In Figs. 7 and 8, the daily battery cycles (at buses 18 and 2, respectively) for the average day of each season are presented. Night-charging batteries (bus 18) are mostly active in the summer and fall (Fig. 7), which is not the case in Fig. 8 for the day-charging batteries (bus 2). Both battery types, however, seem to function only at distinctive time intervals.

## Conclusion

The main contribution of this paper is that it introduces the simultaneous capacity optimization problem of DG and storage in grid-connected and standalone microgrids. More specifically, a methodology has been proposed to optimally integrate DG and energy storage units in microgrids operated either grid-connected or standalone. Simulation results were presented and discussed for a 31-bus medium voltage microgrid, considering grid-connected and standalone operation. The microgrid can contain two types of distributed resources: dispatchable (biomass and battery) and non-dispatchable units (WT and PV). It was found that the more distributed resources are put, the better the performance of the system, since, depending on the selected objective function, the total annual energy losses of the microgrid are minimized or the cost of energy is minimized. Additionally, the power exchange between the microgrid and the main grid is also highly reduced, as the DG and storage units make the microgrid much more autonomous. The maximum reduction in the total annual energy losses of the microgrid or in the cost of energy can be achieved in its grid-connected operation. The results show that, among the four different distributed resources considered (WT, PV, biomass, and battery), the most effective and necessary element for the standalone microgrid are the battery energy storage systems, while the necessary DG units are coming after in terms of priority.

## Acknowledgements

This work has been performed within the European Commission (EC) funded SuSTAINABLE project (contract number FP7-ENERGY-2012.7.1.1-308755). The authors wish to thank the SuSTAINABLE partners for their contributions and the EC for funding this project.

## References

[1] Kuznetsova E, Ruiz C, Li YF, Zio E. Analysis of robust optimization for decentralized microgrid energy management under uncertainty. Int J Electr Power Energy Syst 2015;64:815–32.
[2] Georgilakis PS, Hatziargyriou ND. Optimal distributed generation placement in power distribution networks: Models, methods, and future research. IEEE Trans Power Syst 2013;28:3420–8.
[3] Evangelopoulos VA, Georgilakis PS. Optimal distributed generation placement under uncertainties based on point estimate method embedded genetic algorithm. IET Gener Transm Distrib 2014;8:389–400.
[4] Katsigiannis YA, Georgilakis PS. Effect of customer worth of interrupted supply on the optimal design of small isolated power systems with increased renewable energy penetration. IET Gener Transm Distrib 2013;7:265–75.
[5] Katsigiannis YA, Georgilakis PS, Karapidakis ES. Hybrid simulated annealing-tabu search method for optimal sizing of autonomous power systems with renewables. IEEE Trans Sustain Energy 2012;3:330–8.
[6] Katsigiannis YA, Georgilakis PS, Karapidakis ES. Multiobjective genetic algorithm solution to the optimum economic and environmental performance problem of small autonomous hybrid power systems with renewables. IET Renew Power Gener 2010;4:404–19.
[7] Hung DQ, Mithulananthan N, Lee KY. Optimal placement of dispatchable and nondispatchable renewable DG units in distribution networks for minimizing energy loss. Int J Electr Power Energy Syst 2014;55:179–86.
[8] Vinothkumar K, Selvan MP. Hierarchical agglomerative clustering algorithm method for distributed generation planning. Int J Electr Power Energy Syst 2014;56:259–69.
[9] Prenc R, Škrlec D, Komen V. Distributed generation allocation based on average daily load and power production curves. Int J Electr Power Energy Syst 2013;53:612–22.
[10] Sajjadi SM, Haghifam MR, Salehi J. Simultaneous placement of distributed generation and capacitors in distribution networks considering voltage stability index. Int J Electr Power Energy Syst 2013;46:366–75.
[11] Mohamed Imran A, Kowsalya M, Kothari DP. A novel integration technique for optimal network reconfiguration and distributed generation placement in power distribution networks. Int J Electr Power Energy Syst 2014;63:461–72.
[12] Zhang J, Fan H, Tang W, Wang M, Cheng H, Yao L. Planning for distributed wind generation under active management mode. Int J Electr Power Energy Syst 2013;47:140–6.
[13] Abdi Sh, Afshar K. Application of IPSO-Monte Carlo for optimal distributed generation allocation and sizing. Int J Electr Power Energy Syst 2013;44:786–97.
[14] Ugranli F, Karatepe E. Multiple-distributed generation planning under load uncertainty and different penetration levels. Int J Electr Power Energy Syst 2013;46:132–44.
[15] Crossland AF, Jones D, Wade NS. Planning the location and rating of distributed energy storage in LV networks using a genetic algorithm with simulated annealing. Int J Electr Power Energy Syst 2014;59:103–10.
[16] Jamian JJ, Mustafa MW, Mokhlis H, Baharudin MA. Simulation study on optimal placement and sizing of battery switching station units using artificial bee colony algorithm. Int J Electr Power Energy Syst 2014;55:592–601.
[17] Atwa YM, El-Saadany EF. Optimal allocation of ESS in distribution systems with a high penetration of wind energy. IEEE Trans Power Syst 2010;25:1815–22.
[18] Aghamohammadi MR, Abdolahinia H. A new approach for optimal sizing of battery energy storage system for primary frequency control of islanded microgrid. Int J Electr Power Energy Syst 2014;54:325–33.
[19] Jia H, Mu Y, Qi Y. A statistical model to determine the capacity of battery–supercapacitor hybrid energy storage system in autonomous microgrid. Int J Electr Power Energy Syst 2014;54:516–24.
[20] Zhou W, Lou C, Li Z, Lu L, Yang H. Current status of research on optimum sizing of stand-alone hybrid solar–wind power generation systems. Appl Energy 2010;87:380–9.
[21] Atwa YM, El-Saadany EF, Salama MMA, Seethapathy R. Optimal renewable resources mix for distribution system energy loss minimization. IEEE Trans Power Syst 2010;25:360–70.
[22] Atwa YM, El-Saadany EF. Probabilistic approach for optimal allocation of wind-based distributed generation in distribution systems. IET Renew Power Gener 2011;5:79–88.
[23] Turitsyn K, Sulc P, Backhaus S, Chertkov M. Options for control of reactive power by distributed photovoltaic generators. Proc IEEE 2011;99:1063–73.
[24] Gabash A, Li P. Active–reactive optimal power flow in distribution networks with embedded generation and battery storage. IEEE Trans Power Syst 2012;27:2026–35.
[25] Ochoa LF, Padilha-Feltrin A, Harrison GP. Time-series-based maximization of distributed wind power generation integration. IEEE Trans Energy Convers 2008;23:968–74.
[26] Ochoa LF, Harrison GP. Minimizing energy losses: optimal accommodation and smart operation of renewable distributed generation. IEEE Trans Power Syst 2011;26:198–205.
[27] Lambert T, Gilman P, Lilienthal P. Micropower system modeling with HOMER. In: Farret FA, Simões MG, editors. Integration of alternative sources of energy. Hoboken (NJ): Wiley; 2006. p. 379–418.
[28] GAMS Development Corporation. GAMS — the solvers manual. Washington, DC: GAMS; 2012.
[29] Boggs PT, Tolle JW. Sequential quadratic programming. Acta Numerica 1995;4:1–51.
[30] Nocedal J, Wright SJ. Numerical optimization. 2nd ed. New York: Springer; 2006.
[31] Harrison GP, Piccolo A, Siano P, Wallace AR. Hybrid GA and OPF evaluation of network capacity for distributed generation connections. Electr Power Syst Res 2008;78:392–8.
[32] Teng JH, Luan SW, Lee DJ, Huang YQ. Optimal charging/discharging scheduling of battery storage systems for distribution systems interconnected with sizeable PV generation systems. IEEE Trans Power Syst 2013;28:1425–33.